ACS APPLIED MATERIALS & INTERFACES

www.acsami.org

Research Article

Single-Layered Graphene/Au-Nanoparticles-Based Love Wave Biosensor for Highly Sensitive and Specific Detection of *Staphylococcus aureus* Gene Sequences

Junwang Ji, Yiquan Pang, Dongxiao Li, Xiaoli Wang, Yi Xu,* and Xiaojing Mu*

Cite This: *ACS Appl. Mater. Interfaces* 2020, 12, 12417−12425

Read Online

ACCESS | Metrics & More | Article Recommendations | Supporting Information

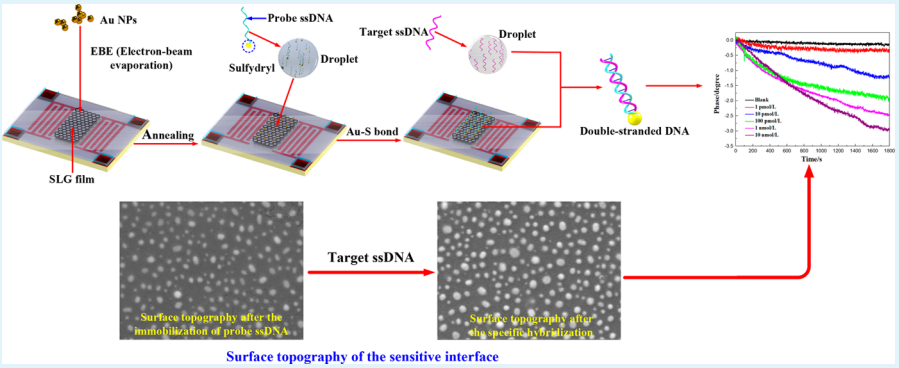

ABSTRACT: In this work, a single-layered graphene (SLG)/Au-nanoparticles (NPs)-based Love wave biosensor was prepared for detection of *Staphylococcus aureus* (*S. aureus*) gene sequences. The annealing process was proposed to obtain a larger-area interface with ssDNA. The sensitivity was verified by detecting *S. aureus* gene sequences with a linear detection ranging from 0 to 10 nmol/L, where the limit of detection (LOD) was only 12.4 pg/mL. The stable state of the biosensors based on SLG/Au NPs in the liquid phase could be kept for more than 0.5 h (±0.1°), and the specificity was verified by detecting noncomplementary ssDNA and one- and three-base mismatched ssDNA. The results of our study suggest that a Love wave biosensor based on SLG/Au NPs hold great potential in clinical testing and diagnosis.

KEYWORDS: *biosensor, chemical vapor deposition, SLG/Au NPs, electron beam evaporation, Staphylococcus aureus gene sequence*

1. INTRODUCTION

As one of the most common pathogens in the human body, *Staphylococcus aureus (S. aureus)* can cause localized purulent infection, pseudomembranous colitis, pneumonia, and even some systemic infections.[1] In addition, *S. aureus* can also cause staphylococcal food poisoning, which is regarded as one of the major foodborne illnesses in the world.[2] Currently, common detection methods of *S. aureus* include enzyme-linked immunosensor assay, real-time polymerase chain reaction (PCR),[3] metal−organic frameworks,[4] magnetic particle enhanced surface plasmon spectroscopy,[5] polydopamine-modified magnetic nanoparticles,[6] and optical and electrochemical biosensors.[7−9] However, these methods have some limitations, such as high costs, requiring expensive precision instruments and professional operators, and long processing times, requiring labeled markers. Therefore, the demand for low costs and operationally simple, rapid, and label-free detection methods is urgently increasing.

In the past decade, surface acoustic wave (SAW)-based sensors were applied in various fields, such as sensors to differentiate a liquid's viscosity and density and a pressure sensor for a harsh environment.[10,11] In addition, types of SAW biosensors have been investigated for detecting various biological samples such as DNA,[12] carcinoembryonic antigens (CEA),[13] and cells.[14] A SAW-based biosensor is favored because of its low cost and high sensitivity, which has great application potential in label-free biodetection and real-time monitoring. Of the different SAW sensors, the Love wave sensor is especially applicable to biological detection in the liquid phase. By deposition of a low-velocity waveguide layer on the surface of a SH-SAW device, the wave energy can be confined to the surface to the largest degree so as to obtain the highest mass sensitivity.[15,16] This accounts for why the Love wave biosensor is better in sensitivity than a quartz crystal

Received: November 13, 2019
Accepted: January 24, 2020
Published: January 24, 2020

https://dx.doi.org/10.1021/acsami.9b20639
ACS Appl. Mater. Interfaces 2020, 12, 12417−12425

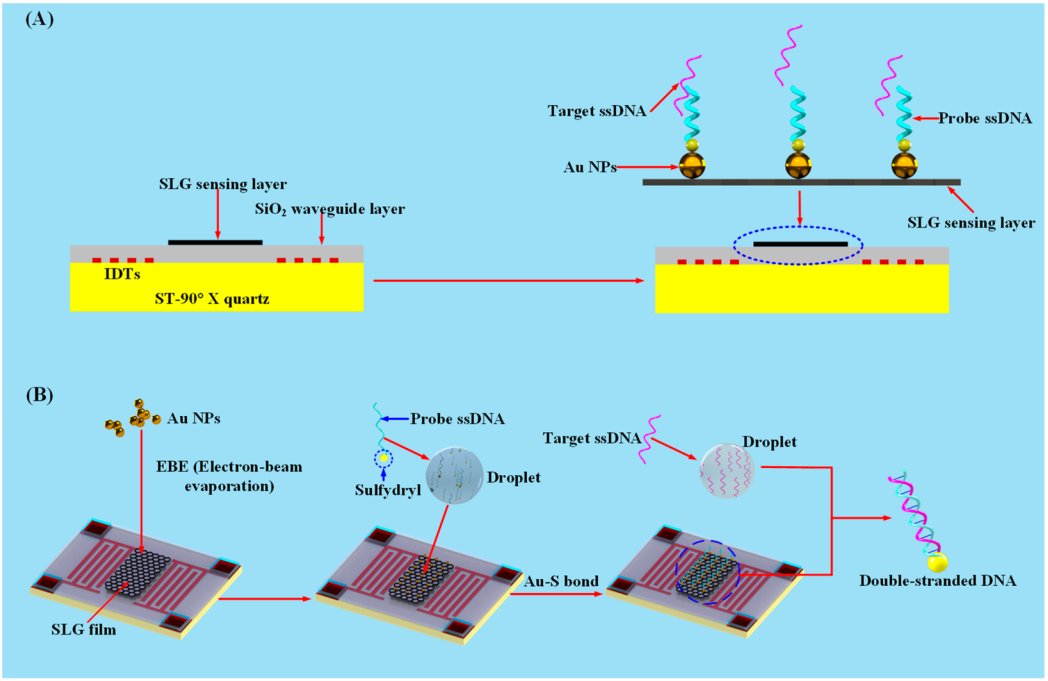

Figure 1. Working principles of a Love wave biosensor and the schematic illustration of *S. aureus* gene sequence detection.

microbalance[17] and LSAW biosensors.[18] However, it has been reported that novel materials and new detection strategies could be employed to further enhance the sensitivity of the Love wave biosensor.

The thickness of the sensitive layer has an important influence on the mass loading of the SAW device.[19] Recently, graphene has attracted great interest from researchers in the biosensor field as it can be used as a sensitive material to enhance the signal of chemo- and biosensors.[20] However, graphene oxide has limited sensitivity because of an unsatisfactory number of layers,[21] and uncontrollable morphology and sample conditions.[22] In contrast, the graphene films prepared by a chemical vapor deposition (CVD) technique have good structural controllability and excellent stability, which is especially suitable for the sensing device.[23] Zheng et al. demonstrated that a small number of graphene layers was beneficial for obtaining higher sensitivity in detection of DNA hybridization.[24] Recent studies also show that the hybrids of Au NPs and graphene can further amplify the signal of a biosensor.[25−28]

In this work, we developed a single-layered graphene (SLG)/Au NPs-based Love wave biosensor for detection of *Staphylococcus aureus* gene sequences. This type of Love wave biosensor was fabricated on a ST-90° X quartz substrate with a base frequency of 282.3 MHz. After that, a CVD-grown SLG film with thickness of 0.3−0.4 nm was deposited onto the surface of a sensitive area, like sensitive film. To obtain a SLG film with dispersed distribution of Au NPs, we adopted electron-beam evaporation (EBE). It is worth noting that the performance of the Love wave biosensor can be decreased if the density of Au NPs is excessively high;[29] annealing was thus proposed to optimize the density of the Au NPs. Figure 1 shows the principles of the proposed Love wave biosensor. Finally, the sensitivity of the proposed biosensor was investigated by linear detection of *S. aureus* gene sequences, and results showed that the limit of detection was as low as 1.86 pmol/L (12.4 pg/mL), indicating excellent sensitivity. In addition, the stability of the proposed biosensor in a liquid was proven; the deviation was lower than 0.1° in 0.5 h. The specificity of the proposed biosensor was verified by detecting noncomplementary ssDNA, one-base mismatched ssDNA, three-base mismatched ssDNA, and target ssDNA, with phase shifts of 0.48°, 1.35°, 1.75°, and 2°, respectively. Therefore, it can be concluded that such proposed biosensor may have great application potential.

2. EXPERIMENTAL SECTION

2.1. Materials and Reagents. The ST-90° X quartz substrates were purchased from Wuxi Haoda Electronics Co., Ltd. The hydrochloric acid, etching solution ($FeCl_3$/HCl), acetone, absolute ethanol, deionized water, and phosphate buffer solution (PBS) were provided by XingHuaGuangBo Chemical Reagent Co., Ltd. (Chongqing, China). The 22-base ssDNA nuc gene sequences are from *S. aureus* O46 chromosome, which are provided by Shanghai Sangon Biological Co., Ltd. The sequences are as follows: Probe ssDNA: 5′-TGGACGTGGCTTAGCGTATATT-3′. Target ssDNA: 5′-AATATACGCTAAGCCACGTCCA-3′. One-base mismatched ssDNA: 5′-AAGATACGCTAAGCCACGTCCA-3′. Three-base mismatched ssDNA: 5′-AAGATACGCTACGCCACGTCTA-3′. Noncomplementary ssDNA: 5′-GCGGTTGAATCGGCGATGGGTG-3′.

PCR experiment was carried out using the Applied Biosystems PCR system (2720 thermal cycler, Applied Biosystems, USA) and the oligonucleotide primers used are as follows: Primer F: 5′-CCTGAAGCAAGTGCATTTACGA-3′. Primer R: 5′-CTTTAGCCA AGCCTTGACGAACT-3′.

2.2. Fabrication of a Love Wave Biosensor. The Love wave biosensors were prepared by the typical Micro Electromechanical System process (Figure S1)[30] with ST-90° X cut quartz used as the piezoelectric substrate because of the excellent stability. SiO_2, which was adopted as the waveguide material in this study, has excellent chemical stability and degradation resistance.[31,32]

First, 4-in. single-side polished quartz wafers with a thickness of 0.5 mm were cleaned to remove the organics and metal ions on the surface. Then the photoresist was applied onto the polished surface by spin coating and the wafer was baked at 90 °C for 30 min. After that, the coated wafer was masked and subjected to the broadband UV light exposure before undergoing hard baking. Subsequently, the wafer

https://dx.doi.org/10.1021/acsami.9b20639
ACS Appl. Mater. Interfaces 2020, 12, 12417−12425

was immersed in developer solution to develop the patterns, followed by cleaning with deionized water and drying with a wafer dryer. Then magnetron sputtering was used to obtain a wafer with Au film (100 nm) fully sputtered. Simultaneously, a 40 nm Cr film was used to increase the surface adhesion of the Au film. At last, the wafer was immersed in the acetone solution and then placed in an ultrasonic cleaner, which aimed at lifting off the metal. For maximum mass sensitivity, the thickness of the SiO_2 waveguide layer was 2 μm.[33] After the IDTs patterns were fabricated, plasma-enhanced chemical vapor deposition (PECVD) was conducted to deposit the waveguide layer onto the wafer to confine the wave energy to the sensing surface and obtain high mass sensitivity. To guarantee the contact between the four pads and the spring probe electrode, the open contact pads were fabricated by reactive ion etching. The spectrogram and parameters of the Love wave device are shown in parts (A) and (B), respectively, of Figure S2.

2.3. Simulation and Verification of the Love Wave. The proposed SLG/Au NPs-based Love wave biosensor consists of a ST-90° X quartz substrate (0.5 mm in thickness) and a SiO_2 waveguide layer (with a thickness of 2 μm). Finite element analysis was performed to investigate the characteristics of the proposed Love wave biosensor using COMSOL 5.2a software in three-dimensional piezoplane strain mode.

2.4. Fabrication of the Detection Cell. To guarantee the Love wave biosensor working in the stable closed environment, a detection cell was fabricated with poly(methyl methacrylate) (PMMA) (Figure S2). The detection cell consisted of chip groove, inlets and outlets, and electrical connectors. For prevention of any leakage of the liquid, a poly(dimethylsiloxane) chip was designed and fabricated. The volume of the liquid cavities is about 15 μL.

2.5. Growth and Transfer of High-Quality SLG Film. In this study, the CVD single-layered graphene was grown on Cu foil (Changda, 99.8% purity), which was placed in the quartz tube. To keep the quartz tube at atmospheric pressure, the tube was then kept sealed and vacuumed with hydrogen gas (H_2) passing into it. To keep the vacuum pump working with constant pressure (100 Pa), the air in the airway should be exhausted three times. After that, the system was heated to 1050 °C in 100 min with a H_2 flow of 20 sccm, and then held for 10 min. A CH_4 flow of 35 sccm was then introduced into the system and held for 20 min. Finally, the SLG film was grown on the surface of Cu foil.

Prior to the transfer of graphene onto the SiO_2 waveguide layer of the biosensor, one side of the copper coil was treated with plasma to clean up the graphene to enhance the corruption of it. Next, via spin coating, PMMA was applied onto graphene on the other side of the copper foil at a spin speed of 3000 rpm for 1 min and then at 1000 rpm for another 1 min. After that, the PMMA layer was baked and the copper foil was immersed in etching solution ($FeCl_3$/HCl) for 0.5 h before the graphene/PMMA was transferred to a rinse bath of isopropanol alcohol and to the SiO_2 waveguide layer successively. Subsequently, the sample was dried in a N_2 atmosphere, baked in air on a hot plate at 60 °C for 2 h, and washed with hot acetone (25 °C) to remove PMMA after cooling down. After the sample had cooled, the PMMA was removed using hot acetone (25 °C). The high-quality SLG film was then obtained in the sensitive area of a Love wave biosensor.

2.6. Evaporation of Au NPs onto the CVD-Grown SLG Film. To immobilize the probe ssDNA in the sensitive area, electron-beam evaporation (EBE) was adopted to uniformly and dispersely load Au NPs onto the CVD-grown SLG film at a rate of 0.1 Å/s. To increase the binding interface for the probe ssDNA and the Au NPs, an annealing process at 700 °C was chosen before the application. Thus, Au NPs with an ideal size were obtained. Additionally, the annealing process could decrease the density of Au NPs, which would promote the performance of the biosensor.

2.7. Material Characterization. The chemical composition of graphene was characterized by X-ray photoelectron spectroscopy (XPS, EscaLab 250Xi, USA). The size of IDTs and the surface topography of SLG in the sensitive area were characterized using a thermal field emission scanning electron microscope (TFESEM, JSM-7800M, Japan). A Raman spectrometer (Renishaw plc, Invia Reflex, UK) was used to collect the Raman spectra of SLG. A transmission electron microscope (TEM, JEM2100F, JEOL, Japan) was used to characterize the SLG sample.

2.8. Procedures of PCR. A bacterial culture was gathered in a 2 mL centrifuge tube for centrifugal treatment at 12000 rpm for 30 s before removal of the supernatant. Subsequently, 150 μL of buffer solution was added into the centrifuge tube containing RNase A, resulting in suspended precipitate. After that, 20 μL of lysozyme stock solution was added to the above solution followed by standing for 5 min, resulting in the solution being used for DNA extraction.

PCR amplification of nucleic acid sequence was conducted in a 0.5 mL sterile centrifuge tube containing 25 μL of solution and transferred to an ice bath. After that, 22 μL of gold mix (green), 1 μL of primer F and primer R (10 pM), 1 μL of DNA template (from 50 ng to 1 μg/μL) were added into the sterile centrifuge tube successively. The experiment started with the denaturation of DNA at 98 °C (120 s), followed by 35 cycles of amplification (98 °C, 10 s; T_m ± 5 °C, 10−15 s; 72 °C, 5−15 s/kb) and final extension at 72 °C (300 s).

2.9. Detection Procedures of *S. aureus* Gene Sequence. Prior to the detection, a Love wave biosensor chip was immersed into absolute alcohol for 60 s, before being washed with deionized water and dried in a N_2 atmosphere. After that, the biosensor chip was placed into the groove of the homemade detection cell (Figure S3D). The phase (P_0) of the Love wave biosensor chip was then monitored until a steady baseline was observed in the air phase. Next, PBS solution was pumped into the reaction cell, which aimed at creating a liquid environment for the biological reactions. During the detection process, the temperature for the detection of *S. aureus* genes was set at 37 °C. Then the steady-state phase was obtained, which is noted as P_1. The probe ssDNA solution at optimal concentration was then pumped into the detection cell, resulting in the steady-state phase P_2. Finally, the target ssDNA solution at various concentrations were respectively pumped into the detection cell and stable state phase P_3 was obtained. Therefore, the phase shift that was ascribed to the DNA hybridization can be calculated by $\Delta P = P_3 - P_2$.

2.10. Specificity Assessment of the Biosensor. For assessment of the specificity of the proposed Love wave biosensor chip, one- and three-base mismatched ssDNA and noncomplementary ssDNA were respectively pumped into the reaction cell to hybridize with the target ssDNA. The phase signals were then monitored and recorded. Therefore, the specificity of the Love wave biosensor could be explored.

2.11. Regeneration of the Biosensor. For investigation of the regeneration of the biosensor, the experiment was repeated under the same concentration as that of the Love wave biosensor chip. The conjugate on the surface of the sensitive area was removed by immersion in ethylenediaminetetraacetic acid solution after each measurement. The obtained biosensor chip was rinsed with PBS buffer three times and then washed with deionized water before being used to detect the *S. aureus* gene sequence. It was worth noting that the detection procedure was repeated five times.

3. RESULTS AND DISCUSSION

3.1. Configuration and Working Principles of a Love Wave Biosensor with Au-NPs-Functionalized SLG film. The detection process of *S. aureus* gene sequences is shown in Figure 1. It is known that the amplitude of the Love wave and phase velocity would change when the mass change occurred on the propagation path. For immobilization of the probe ssDNA in the sensitive area, the gold nanoparticles were deposited onto the SLG film by the EBE process. Prior to the detection, the optimal concentration of the probe ssDNA was obtained by detecting various concentrations of the probe ssDNA solution. After the stable state phase signal was reached, the target ssDNA solution was pumped into the reaction cell (Figure S3). Through observation of the phase

https://dx.doi.org/10.1021/acsami.9b20639
ACS Appl. Mater. Interfaces 2020, 12, 12417−12425

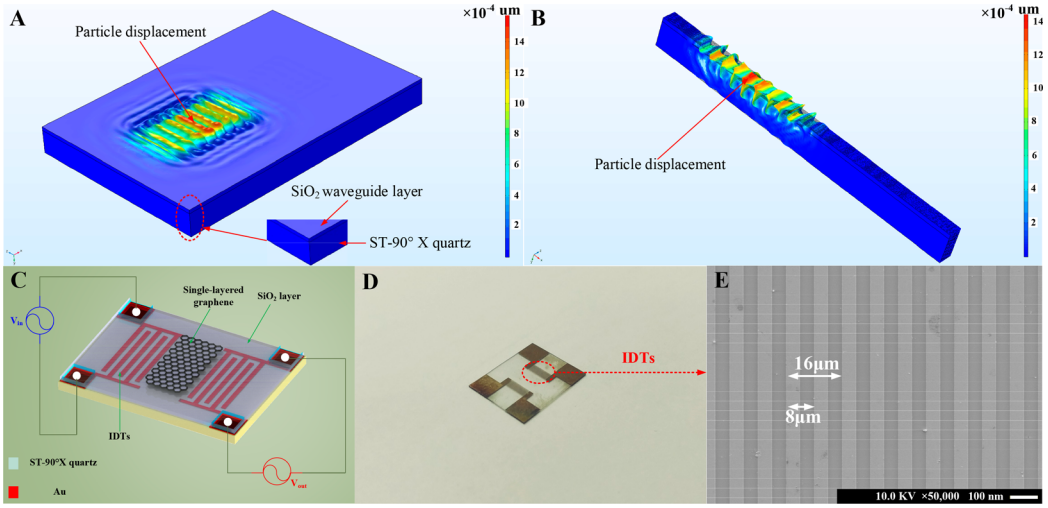

Figure 2. (A) 3D model of the Love wave vibration model. (B) Sectional view of the Love wave vibration model. (C) Schematic of the Love wave biosensor chip. (D) Photograph of a fabricated Love wave biosensor chip. (E) SEM image of the IDTs.

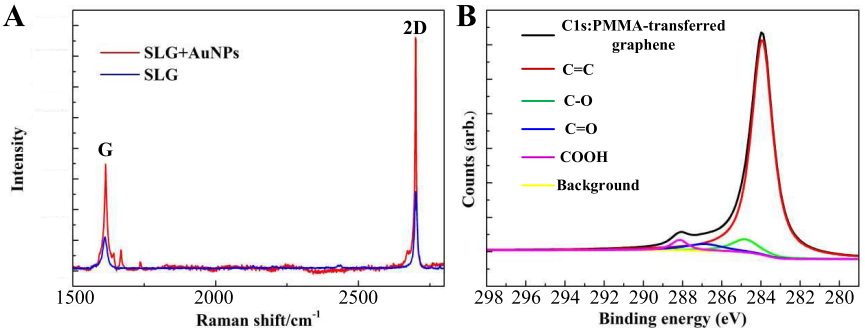

Figure 3. (A) Raman spectra of CVD-grown SLG (blue curve) and gold-nanoparticles-functionalized SLG (red curve). (B) XPS spectra of the C 1s of the CVD-grown SLG film.

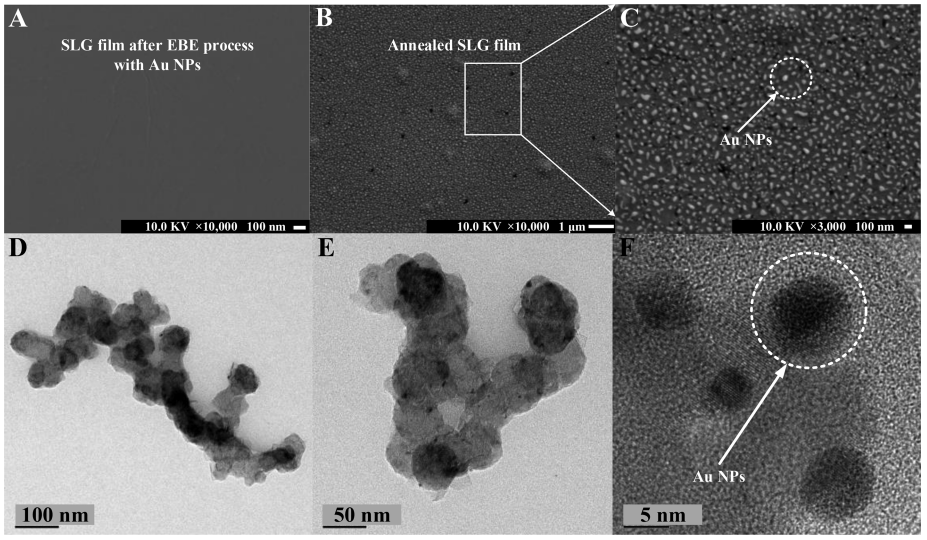

Figure 4. (A) SEM image of CVD-grown SLG film after the EBE process with Au NPs. (B), (C) Surface topography of Au-NPs-functionalized SLG film after annealing at 700 °C. (D)−(F) TEM images of Au-NPs-functionalized SLG film after annealing at 700 °C, which were obtained from the sensitive area of the Love wave biosensor chip.

shift, the phase change could be attributed to the mass change in the sensitive area when the phase signal was once again kept at a stable value.

The propagation of the surface acoustic wave on the SiO_2 waveguide layer is shown in Figure 2.[34] The propagation of the Love wave along the SiO_2 waveguide layer was observed by a 3D model is shown in Figure 2A. The sectional view is shown

https://dx.doi.org/10.1021/acsami.9b20639
ACS Appl. Mater. Interfaces 2020, 12, 12417−12425

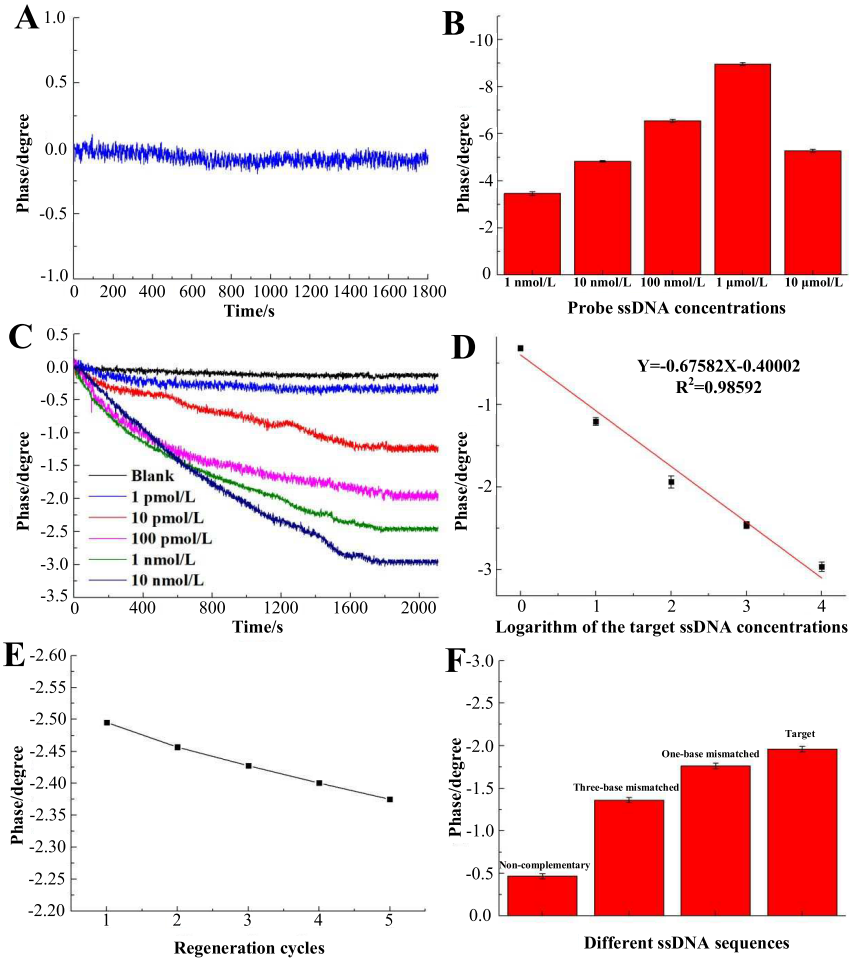

Figure 5. (A) Baseline signal in PBS solution. (B) Picture of the phase shift with various probe concentrations, and the optimal probe concentration was verified to be 1 μmol/L. (C) Phase changes of the specific binding of the probe ssDNA and target ssDNA at different concentrations, which were recorded in real time. (D) Standard curve for the detection of *S. aureus* gene sequence with a Love wave biosensor based on Au-NPs-functionalized SLG film. (E) Relation between sensing activity changes of a Love wave biosensor and number of regeneration cycles. (F) Histogram of the noncomplementary ssDNA, three-base mismatched ssDNA, one-base mismatched ssDNA, and target ssDNA binding with the probe ssDNA, which were all analyzed at a concentration of 1 nmol/L.

in Figure 2B. The schematic diagram of the Love wave biosensor chip is presented in Figure 2C, and the real product of a biosensor chip is shown in Figure 2D. The SEM image (Figure 2E) indicates that the length of one cycle is 16 μm and the width of a single IDT is 4 μm.

3.2. Characterization of the Au-NPs-Functionalized SLG Film. Raman spectroscopy was conducted to examine and analyze the quality of the CVD-grown SLG film. As shown in Figure 3A, the characteristic peak of a high-quality SLG was observed, which corresponds to a sharp G-band (≈1600 cm^{-1}) and a sharp two-dimensional (2D) band (≈2699−2720 cm^{-1}), respectively.[35] In addition, the excellent quality of the SLG was also validated by the I_{2D}/I_G ratio (≈2.4). Also, obvious Raman enhancement can be observed (red curve) after the EBE process with Au NPs. The composition of the SLG film was investigated by XPS. As shown in Figure 3B, the black curve represents the raw spectrum, the red curve represents the sp^2 component of C═C at 284.6 eV, the green curve represents C−O at 286.1 eV, the blue curve represents C═O at 287.1 eV, and the purple curve represents COOH at 288.7 eV.[36] The content of the chemical states of these elements at different peak positions are calculated by the peak area. In addition, the size distribution of the Au NPs was measured by DLS (Figure S4), which shows that the size distribution of the Au NPs is in a narrow range, with 96.8% of the particles' sizes at 18.1 nm.

The surface topography of the sensitive area after the EBE process and annealing was characterized by SEM. As shown in Figure 4A, there is no significant changes in the sensitive area after the EBE process. However, uniformly sized Au NPs formed in the sensitive area (Figure 4B,C) after annealing, indicating an appropriate density of the Au NPs. The Au-NPs-functionalized SLG film was characterized by HRTEM. As shown in Figure 4D−F, the morphology of the Au-NPs-functionalized SLG film can be clearly observed, which indicates that the size and distribution of the gold nanoparticles were uniform.

3.3. Analytical Performance of the Love Wave Biosensor Based on Au-NPs-Functionalized SLG Film. The liquid-phase stability of the Love wave biosensor is of critical importance in gene detection. Prior to the detection, the stability of the Love wave biosensor was verified by pumping PBS solution into the sensitive area. The result (Figure 5A) revealed that the Love wave biosensor in this work had excellent stability. Therefore, the phase shifts can be

https://dx.doi.org/10.1021/acsami.9b20639
ACS Appl. Mater. Interfaces 2020, 12, 12417−12425

attributed to the mass change in the sensitive area, and the authenticity of the data can be guaranteed.

The surface density of the probe ssDNA is a key factor in construction of a sensing layer. For verfication of the impact of probe ssDNA concentration on the phase shift, various concentrations of probe ssDNA were respectively immobilized on the surface of the sensitive area and then the biosensors were respectively placed into the detection cells for reaction. The results revealed that the phase shifts significantly decreased with the gradual increase of the probe ssDNA concentration (Figure 5B). The Love wave biosensor in this work displayed optimum sensitivity of the phase response at probe ssDNA concentration of 1 μmol/L.

Under the optimal and stable detection conditions, the performance of the Love wave biosensor with Au-NPs-functionalized SLG film was assessed by detecting various concentrations of the target ssDNA (blank, 1 pmol/L, 10 pmol/L, 100 pmol/L, 1 nmol/L, and 10 nmol/L). As shown in Figure 5C, the phase shifts linearly increased as the target ssDNA concentration increased from blank to 10 nmol/L. The linear regression equation utilized to calculate the phase shifts is $Y = -0.67582X - 0.40002$, in which X represents the logarithm of the target ssDNA concentrations (Figure 5D). In addition, Langmuir isothermal theory, $Y = \frac{qkX}{1+kX}$, was used to fit the calibration curve.[38,39] The corresponding fitting equation (R_2 = 0.95309) for the Au NPs/SLG is $Y = -1.4755X/1 + 0.25621X$ (Figure S5).

The limit of detection (LOD) can be calculated by the following equation

$$\mathrm{LOD} = \frac{3\sigma}{S} \quad (1)$$

where σ is the standard deviation (SD) and S is the mean slope of the linear regression equation. In this work, the LOD was as low as 1.86 pmol/L, which was set at 3-fold SD above the blank.[37] Table 1 shows the relative standard deviations of phase signals of different concentrations of *S. aureus* gene sequences. The experiment results were also compared with some other reported results in Table 2. Besides that, the regeneration of the Love wave biosensor was assessed by repeating the same detection procedure five times, which were performed after removal of the nucleic acid conjugate from the sensitive area. The result (Figure 5E) revealed that the sensing activity of the proposed Love wave biosensor maintained 94% of the original activity after five regeneration cycles, indicating excellent repeatability. The stability of the proposed Love wave biosensor was investigated by storing it at 4 °C for 20 days. Results showed that the Δphase accounted for 80% of the initial Δphase, indicating satisfactory stability (Figure 6).

Table 1. Relative Standard Deviation of Phase Signals Obtained from Different *S. aureus* Gene Sequence Concentrations

RSD of different *S. aureus* gene sequence concentrations (%)				
1 pmol/L	10 pmol/L	100 pmol/L	1 nmol/L	10 nmol/L
10.76	3.90	3.79	7.4	1.83

The specificity of the biosensor is of vital importance in detection of *S. aureus* gene sequences. Using the non-complementary ssDNA alone may cause a higher phase shift than the actual value, which would lead to a false phase signal response. In this work, noncomplementary ssDNA, three-base mismatched ssDNA, one-base mismatched ssDNA, and target ssDNA were separately pumped into the detection cell to react with the probe ssDNA, with the aim of validating the specificity of the proposed Love wave biosensor. As shown in Figure 5F, the phase shift of the noncomplementary ssDNA was lower than 0.5°, which was significantly lower than that of the three-base mismatched ssDNA, and the phase shift of the target ssDNA (2°) was higher than that of the one-base mismatched ssDNA and three-base mismatched ssDNA, which indicates sound specificity of the proposed Love wave biosensor.

After recycling, the PCR product was diluted with PBS solution, followed by heating in a water bath at 100 °C for 10 min and cooling in an ice bath for 2 min. The resulting ssDNA sample solution (10 nmol/L) was added into the reaction cell to react with the probe ssDNA for detection of *S. aureus* gene sequences. As shown in Figure 7, the Δphase was about 9° after the immobilization of probe ssDNA, which then decreased to about 3° after the hybridization with the PCR product, suggesting the formation of dsDNA at the sensitive area interface. Therefore, the proposed method is expected to be an effective approach for detection of the target ssDNA sequence.

The SEM images are presented in Figure 8, which are used to characterize the surface morphology changes of the sensitive area in the detection procedure. As is shown in Figure 8A,B, the appearance/size of the annealed Au NPs are irregular. After the probe ssDNA was immobilized on the surface of the sensitive film, the surface morphology of the sensitive area with Au-NPs-functionalized SLG film and appearance/size of the Au NPs changed significantly (Figure 8C, D), which indicates that probe ssDNA has bound to the Au NPs by Au−S bonds. After the target ssDNA was pumped into the detection cell, the significant change of the surface morphology (Figure 8E,F) demonstrates that the specific hybridization of the probe ssDNA and the target ssDNA has occurred. Additionally, the AFM images are shown in Figure S6.

4. CONCLUSIONS

In this work, a novel SLG/Au NPs-based Love wave biosensor was fabricated for detection of *S. aureus* gene sequences. The design and fabrication of a homemade detection cell increased the ease of the operation. Moreover, this strategy was proved

Table 2. Comparison of the Sensitivity and the LOD to Other Reported Studies

methods	materials	detection	linear range	LOD	references
Love wave	Au NPs	CEA	10 pg/mL to 10 ng/mL	37 pg/mL	13
SH-SAW	gold	*Pseudomonas aeruginosa* gene sequences	0.1−1000 nmol/L	9.5 ng/mL	12
SH-SAW	gold	single-stranded DNA	1.3−130 nmol/L	1.8 ng/mL	40
Hall effect	SLG/Au NPs	single-stranded DNA	1 pM to 100 nM	1 pM	28
Love wave	SLG/Au NPs	*S. aureus* gene sequences	0−10nmol/L	12.4 pg/mL	this work

https://dx.doi.org/10.1021/acsami.9b20639
ACS Appl. Mater. Interfaces 2020, 12, 12417−12425

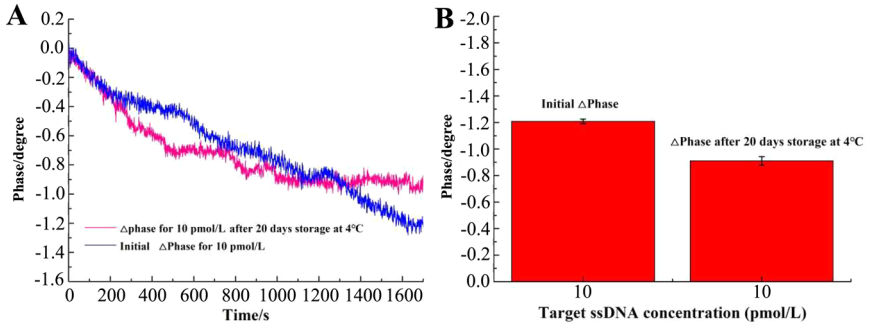

Figure 6. (A) Initial Δphase (blue curve) and the Δphase after 20 days of storage at 4 °C (pink curve). (B) Corresponding histogram of the Δphase signals.

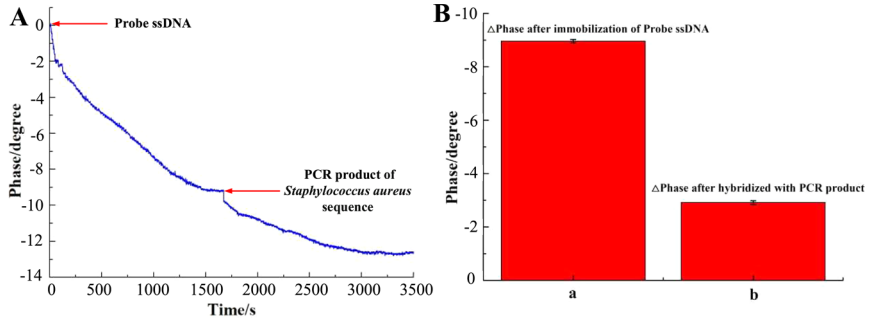

Figure 7. (A) Whole detection process of the hybridization of probe ssDNA and PCR product of *S. aureus* sequence. (B) Corresponding histogram of the Δphase signals.

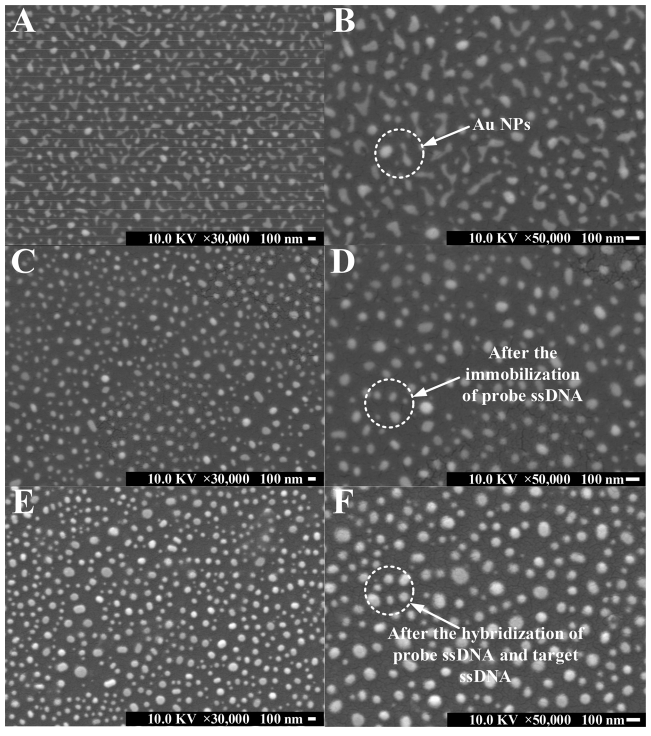

Figure 8. (A), (B) Surface morphology of the sensitive area after the annealing process. (C), (D) Surface morphology of the sensitive area after the immobilization of probe ssDNA. (E), (F) Surface morphology of the sensitive area after the hybridization of probe ssDNA and target ssDNA.

to be an effective platform for the detection of *S. aureus* gene sequences with a limit of detection of 1.86 pmol/L (12.4 pg/mL). With excellent stability and repeatability, the proposed Love wave biosensor has promising application potential in detection of *S. aureus* gene sequences. Therefore, the SLG/Au-NPs-based Love wave biosensor may provide more rapid and effective quantification of biological samples at low concentrations.

■ ASSOCIATED CONTENT

Supporting Information

The Supporting Information is available free of charge at https://pubs.acs.org/doi/10.1021/acsami.9b20639.

Fabrication processes, spectrogram of a Love wave biosensor, SEM image of the IDTs, and structure of a detection cell; the calibration curve for the detection of *S. aureus* gene sequences and nanoparticle sizes measured by DLS (PDF)

■ AUTHOR INFORMATION

Corresponding Authors

Xiaojing Mu − *Key Laboratory of Optoelectronic Technology & Systems, Ministry of Education, International R & D Center of Micro-nano Systems and New Materials Technology, College of Optoelectronic Engineering, Chongqing University, Chongqing 400044, China;* orcid.org/0000-0003-2024-2595; Email: mxjacj@cqu.edu.cn

Yi Xu − *Key Laboratory of Optoelectronic Technology & Systems, Ministry of Education, International R & D Center of Micro-nano Systems and New Materials Technology, College of Optoelectronic Engineering, Chongqing University, Chongqing 400044, China;* orcid.org/0000-0002-7037-0985; Email: xuyibbd@cqu.edu.cn

https://dx.doi.org/10.1021/acsami.9b20639
ACS Appl. Mater. Interfaces 2020, 12, 12417−12425

Authors

Junwang Ji − *Key Laboratory of Optoelectronic Technology & Systems, Ministry of Education, International R & D Center of Micro-nano Systems and New Materials Technology, College of Optoelectronic Engineering, Chongqing University, Chongqing 400044, China*

Yiquan Pang − *School of Chemistry and Chemical Engineering, Chongqing University, Chongqing 400030, China*

Dongxiao Li − *Key Laboratory of Optoelectronic Technology & Systems, Ministry of Education, International R & D Center of Micro-nano Systems and New Materials Technology, College of Optoelectronic Engineering, Chongqing University, Chongqing 400044, China*

Xiaoli Wang − *Key Laboratory of Optoelectronic Technology & Systems, Ministry of Education, International R & D Center of Micro-nano Systems and New Materials Technology, College of Optoelectronic Engineering, Chongqing University, Chongqing 400044, China*

Complete contact information is available at: https://pubs.acs.org/10.1021/acsami.9b20639

Notes

The authors declare no competing financial interest.

■ ACKNOWLEDGMENTS

This study was supported by the National Natural Science Foundation of China (Grant No. 51605060), the National Key Research and Development Program of China (Grant No. 2016YFB0402702), the Fundamental Research Funds for the Central Universities (No. 2018CDPTCG0001-5), and Chongqing Municipality Key Research and Development Program of China (Grant No. cstc2017rgzn-zdyfX0041).

■ REFERENCES

(1) Tong, S. Y. C.; Davis, J. S.; Eichenberger, E.; Holland, T. L.; Fowler, V. G. Staphylococcus aureus Infections: Epidemiology, Pathophysiology, Clinical Manifestations, and Management. *Clin. Microbiol. Rev.* **2015**, *28*, 603−661.

(2) Argudín, M. A.; Mendoza, M. C.; Rodicio, M. R. Food Poisoning and Staphylococcus aureus Enterotoxins. *Toxins* **2010**, *2*, 1751−1773.

(3) Yoon, J. H.; Wei, S.; Oh, D. H. A Highly Selective Enrichment Broth Combined with Real-time PCR for Detection of Staphylococcus aureusin Food Samples. *LWT - Food Science and Technology.* **2018**, *94*, 103−110.

(4) Bhardwaj, N.; Bhardwaj, S. K.; Mehta, J.; Kim, K. H.; Deep, A. MOF-Bacteriophage Biosensor for Highly Sensitive and Specific Detection of Staphylococcus aureus. *ACS Appl. Mater. Interfaces* **2017**, *9*, 33589−33598.

(5) Rüppel, N.; Tröger, V.; Sandetskaya, N.; Kuhlmeier, D.; Schmieder, S.; Sonntag, F. Detection and Identification of Staphylococcus aureus Using Magnetic Particle Enhanced Surface Plasmon Spectroscopy. *Eng. Life Sci.* **2018**, *18*, 263−268.

(6) Gao, X. M.; Yao, X.; Zhong, Z. T.; Jia, L. Rapid and Sensitive Detection of Staphylococcus aureus Assisted by Polydopamine Modified Magnetic Nanoparticles. *Talanta* **2018**, *186*, 147−153.

(7) Shahdordizadeh, M.; Taghdisi, S. M.; Ansari, N.; Alebooye Langroodi, F.; Abnous, K.; Ramezani, M. Aptamer Based Biosensors for Detection of Staphylococcus aureus. *Sens. Actuators, B* **2017**, *241*, 619−635.

(8) Niu, X. L.; Chen, W.; Wang, X. L.; Men, Y. L.; Wang, Q.; Sun, W.; Li, G. J. A Graphene Modified Carbon Ionic Liquid Electrode for Voltammetric Analysis of the Sequence of the Staphylococcus aureus nuc Gene. *Microchim. Acta* **2018**, *185*, 167−175.

(9) Niu, X. L.; Zheng, W.; Li, X. Y.; Zhao, W. S.; Wen, Z. R.; Li, Q. T.; Xie, H.; Sun, W. Electrochemical DNA Sensor Based on Chitosan-Graphene and Electrodeposited Gold Nanoparticle Modified Electrode for The Detection of Staphylococcus aureus nuc Gene Sequence. *Curr. Anal. Chem.* **2018**, *14* (2), 159−165.

(10) Wang, T.; Mu, X. J.; Kropelnicki, P.; Randles, A. B.; Lee, C. K. Viscosity and Density Decoupling Method Using a Higher Order Lamb Wave Sensor. *J. Micromech. Microeng.* **2014**, *24*, 075002.

(11) Wang, T.; Mu, X. J.; Randles, A. B.; Gu, Y. D.; Lee, C. K. Diaphragm shape effect on the sensitivity of surface acoustic wave based pressure sensor for harsh environment. *Appl. Phys. Lett.* **2015**, *107*, 123501.

(12) Ji, J. W.; Yang, C.; Zhang, F.; Shang, Z. G.; Xu, Y.; Chen, Y.; Chen, M.; Mu, X. J. A High Sensitive SH-SAW Biosensor Based 36° Y-X Black LiTaO3 for Label-free Detection of Pseudomonas Aeruginosa. *Sens. Actuators, B* **2019**, *281*, 757−764.

(13) Li, S. M.; Wan, Y.; Su, Y.; Fan, C. H.; Bhethanabotla, V. R. Gold Nanoparticle-based Low Limit of Detection Love Wave Biosensor for Carcinoembryonic Antigens. *Biosens. Bioelectron.* **2017**, *95*, 48−54.

(14) Chang, K.; Pi, Y.; Lu, W. P.; Wang, F.; Pan, F.; Li, F. K.; Jia, S. R.; Shi, J. F.; Deng, S. L.; Chen, M. Label-free and High-sensitive Detection of Human Breast Cancer Cells by Aptamer-based Leaky Surface Acoustic Wave Biosensor Array. *Biosens. Bioelectron.* **2014**, *60*, 318−324.

(15) McHale, G.; Newton, M. I.; Martin, F.; Gizeli, E.; Melzak, K. A. Resonant Conditions for Love Wave Guiding Layer Thickness. *Appl. Phys. Lett.* **2001**, *79*, 3542−3543.

(16) Harding, G. L.; Du, J.; Dencher, P. R.; Barnett, D.; Howe, E. Love Wave Acoustic Immunosensor Operating in Liquid. *Sens. Actuators, A* **1997**, *61*, 279−286.

(17) Gaso, M. I. R.; Jiménez, Y.; Francis, L. A.; Arnau, A. *Love Wave Biosensors: A Review*; InTech: 2013; pp 277−310.

(18) Trivedi, S.; Nemade, H. B. Finite Element Simulation of Love Wave Resonator for DNA Detection. *Int. J. Adv. Eng. Sci. Appl. Math.* **2015**, *7*, 210−218.

(19) Goto, M.; Yatsuda, H.; Kondoh, J. IUS4-PD-6 Optimization of gold film thickness for SH-SAW biosensor on quartz. Presented at 2013 Joint UFFC, EFTF and PFM Symposium, Prague, Czech Republic, 2013; Paper IUS4-PD-6.

(20) Sharma, P. S.; D'Souza, F.; Kutner, W. Graphene and Graphene Oxide Materials for Chemo- and Biosensing of Chemical and Biochemical Hazards2014. *Top. Curr. Chem.* **2013**, *348*, 237−266.

(21) Muti, M.; Sharma, S.; Erdem, A.; Papakonstantinou, P. Electrochemical Monitoring of Nucleic Acid Hybridization by Single-Use Graphene Oxide-Based Sensor. *Electroanalysis* **2011**, *23*, 272−279.

(22) Liu, Y. X.; Dong, X. C.; Chen, P. Biological and Chemical Sensors Based on Graphene Materials. *Chem. Soc. Rev.* **2012**, *41*, 2283−2307.

(23) Chen, X. P.; Zhang, L. L.; Chen, S. S. Large Area CVD Growth of Graphene. *Synth. Met.* **2015**, *210*, 95−108.

(24) Zheng, C.; Huang, L.; Zhang, H.; Sun, Z.; Zhang, Z.; Zhang, G. J. Fabrication of Ultrasensitive Field-Effect Transistor DNA Biosensors by a Directional Transfer Technique Based on CVD-Grown Graphene. *ACS Appl. Mater. Interfaces* **2015**, *7*, 16953−16959.

(25) Song, Y. C.; Xu, T. L.; Xu, L. P.; Zhang, X. J. Nanodendritic Gold/Graphene-based Biosensor for Tri-mode MiRNA Sensing. *Chem. Commun.* **2019**, *55*, 1742−1745.

(26) Wang, J.; Han, H.; Jiang, X. C.; Huang, L.; Chen, L. N.; Li, N. Quantum Dot-Based Near-Infrared Electrochemiluminescent Immunosensor with Gold Nanoparticle-Graphene Nanosheet Hybrids and Silica Nanospheres Double-Assisted Signal Amplification. *Anal. Chem.* **2012**, *84*, 4893−4899.

(27) Hernandez-Sanchez, D.; Villabona-Leal, G.; Saucedo-Orozco, I.; Bracamonte, V.; Perez, E.; Bittencourt, C.; Quintana, M. Stable Graphene Oxide-Gold Nanoparticle Platforms for Biosensing Applications. *Phys. Chem. Chem. Phys.* **2018**, *20*, 1685−1692.

(28) Loan, P. T. K.; Wu, D.; Ye, C.; Li, X.; Tra, V. T.; Wei, Q.; Fu, L.; Yu, A.; Li, L. J.; Lin, C. T. Hall Effect Biosensors with Ultraclean

Graphene Film for Improved Sensitivity of Label-free DNA Detection. *Biosens. Bioelectron.* **2018**, *99*, 85−91.
(29) Liu, J. X.; Chen, X. H.; Wang, Q. Q.; Xiao, M. M.; Zhong, D. L.; Sun, W.; Zhang, G. Y.; Zhang, Z. Y. Ultrasensitive Monolayer MoS2 Field-Effect Transistor Based DNA Sensors for Screening of Down Syndrome. *Nano Lett.* **2019**, *19*, 1437−1444.
(30) Rana, L.; Gupta, R.; Tomar, M.; Gupta, M. Highly Sensitive Love Wave Acoustic Biosensor for Uric Acid. *Sens. Actuators, B* **2018**, *261*, 169−177.
(31) Ballantine, D. S.; White, R. M.; Martin, S. J.; Ricco, A. J.; Zellers, E. T.; Frye, G. C.; Wohltjen, H. *Acoustic Wave Sensors: Theory, Design, and Physico-Chemical Applications*; Academic Press: 1997.
(32) Li, S.; Sankaranarayanan, S. K. R. S.; Fan, C.; Su, Y.; Bhethanabotla, V. R. Achieving Lower Insertion Loss and Higher Sensitivity in A SAW Biosensor Via Optimization of Waveguide and Microcavity Structures. *IEEE Sens. J.* **2017**, *17*, 1608−1616.
(33) Caliendo, C.; Hamidullah, M. Guided Acoustic Wave Sensors for Liquid Environments. *J. Phys. D: Appl. Phys.* **2019**, *52*, 153001.
(34) Han, K.; Yuan, Y. J. Mass Sensitivity Evaluation and Device Design of a LOVE Wave Device for Bond Rupture Biosensors Using the Finite Element Method. *IEEE Sens. J.* **2014**, *14*, 2601−2608.
(35) Malard, L. M.; Pimenta, M. A.; Dresselhaus, G.; Dresselhaus, M. S. Raman Spectroscopy in Graphene. *Phys. Rep.* **2009**, *473*, 51−87.
(36) Poh, H. L.; Sanek, F.; Ambrosi, A.; Zhao, G.; Sofer, Z.; Pumera, M. Graphenes Prepared by Staudenmaier, Hofmann and Hummers Methods with Consequent Thermal Exfoliation Exhibit Very Different Electrochemical Properties. *Nanoscale* **2012**, *4*, 3515−3522.
(37) Long, G. L.; Winefordner, J. D. Limit of Detection. A Closer Look at the IUPAC Definition. *Anal. Chem.* **1983**, *55*, 712A−724A.
(38) Langmuir, I. The Adsorption of Gases on Plane Surfaces of Glass, Mica, and Platinum. *J. Am. Chem. Soc.* **1918**, *40*, 1361−1403.
(39) Langmuir, I. The Constitution and Fundamental Properties of Solids and Liquids. Part I. Solids. *J. Am. Chem. Soc.* **1916**, *38*, 2221−2295.
(40) Cai, H. L.; Yang, Y.; Zhang, Y. H.; Zhou, C. J.; Guo, C. R.; Liu, J.; Ren, T. L. A High Sensitivity Wireless Mass-loading Surface Acoustic Wave DNA Biosensor. *Mod. Phys. Lett. B* **2014**, *28*, 1450056.

https://dx.doi.org/10.1021/acsami.9b20639
ACS Appl. Mater. Interfaces 2020, 12, 12417−12425